

Magic radioactivity of ^{252}Cf

M. Mirea¹, D.S. Delion^{1,2} and A. Săndulescu^{2,3}

¹*National Institute of Physics and Nuclear Engineering,
407 Atomistilor, 077125 Bucharest-Măgurele, Romania*

²*Academy of Romanian Scientists*

³*54 Splaiul Independenței, 050094 Bucharest, Romania*

³*Institute for Advanced Studies in Physics,
129 Calea Victoriei, Bucharest, Romania*

We show that the sharp maximum corresponding to ^{107}Mo in the fragment distribution of the ^{252}Cf cold fission is actually a Sn-like radioactivity, similar to other decay processes in which magic nuclei are involved, namely α -decay and heavy cluster emission, also called Pb-like radioactivity. It turns out that the mass asymmetry degree of freedom has a key role in connecting initial Sn with the final Mo isotopes along the fission path. We suppose the cold rearrangement of nucleons within the framework of the two center shell model, in order to compute the cold valleys in the charge equilibrated fragmentation potential. The fission yields are estimated by using the semiclassical penetration approach. We consider five degrees of freedom, namely the inter-fragment distance, the shapes of fragments, the neck parameter and mass asymmetry. We found an isomeric minimum between the internal and external barriers. It turns out that the inner cold valley of the total potential energy is connected to the double magic isotope ^{132}Sn .

The spontaneous cold rearrangement of nucleons from an initial nucleus to two final fragments corresponds to the most favorable path of the cold splitting in the potential energy surface [1]. This path, called cold valley, is related to the magicity of one or both fission fragments. Thus, α -decay is connected to the cold valley of the double magic nucleus ^4He . The cold valley of the double magic ^{208}Pb is responsible for various heavy cluster decays, in which C, O, Ne, Mg and Si are emitted [2] and this is the reason why they are also called "magic-radioactivities".

On the other hand the production of superheavy elements is connected with the inverse fusion process [3], involving double magic nuclei ^{208}Pb and ^{48}Ca [4, 5].

Two main synthesis procedures of superheavy nuclei based on fusion reactions have been experimentally used:

(a) the cold-fusion at GSI Darmstadt with either ^{208}Pb or ^{209}Bi target leading to a small excitation energy of the compound nucleus followed by a single neutron evaporation [6, 7], and

(b) the hot fusion with ^{48}Ca projectile at JINR Dubna, in which the compound nucleus is very excited hence more neutrons are evaporated [3, 8].

Almost two decades ago, systematic measurements were performed to determine cold fission yields of ^{252}Cf [9, 10]. The aim of this work is to analyze these data and to show that the cold fission of ^{252}Cf is strongly connected with the cold valley of the double magic isotope ^{132}Sn , although the experimental cold yields have a maximum corresponding to a different charge number.

In the past the cold fission of ^{252}Cf was investigated within the double folding potential method [11, 12] emphasizing the role of higher deformations. In Ref [13], based on a macroscopic model by determining the tip distances for the exit point from the barrier for ground state deformed fragments, it was predicted that the major contribution in the yield distribution corresponds to

the light fission fragment $A_2 \approx 100$, contradicting experimental data showing a peak at $A_2 = 107$. In this study we explain the root of this discrepancy.

We extend the analysis performed in Ref. [14] to a more reliable microscopic approach to estimate the fission barrier, based on a new version of the Super Asymmetric Two Center Shell Model [15]. This approach was already used to describe the fusion/fission of some superheavy elements [16] and of the dynamical effects in fission [15, 17].

In this work the nuclear shape parametrization is obtained by smoothly joining two spheroids with a third surface, given by the rotation of a circle around the symmetry axis. This parametrization is characterized by 5 degrees of freedom, namely the mass asymmetry, the elongation $R = z_2 - z_1$ given by the distance between the centers of the nascent fragments, the two deformations of the nascent fragments associated to the eccentricities $\varepsilon_i = \sqrt{1 - b_i^2/a_i^2}$ ($i=1,2$), and the necking characterized by the curvature $C = S/R_3$ of the median surface and a asymmetry term given by the ratio of the semi-axis $\eta = a_1/a_2$. In this parametrization the values $S=1$ and $S=-1$ stand for necked and swollen shapes in the median surface, respectively. Within these generalized coordinates, for necked shapes it is possible to estimate the mass of the nascent fragment A_2 during the deformation.

The penetrability, corresponding to some binary partition, defines the isotopic yield. This quantity can be estimated by using the semiclassical integral [18]

$$P_{A_2} = \exp \left\{ -2 \int_{R_1}^{R_2} \sqrt{\frac{2M(A_2, R)}{\hbar^2} V(A_2, R)} dR \right\}, \quad (1)$$

between internal and external turning points along a fission path. Two ingredients are mandatory in order to evaluate the action integral: the inertial parameter M and the fragmentation deformation energy V (we will call

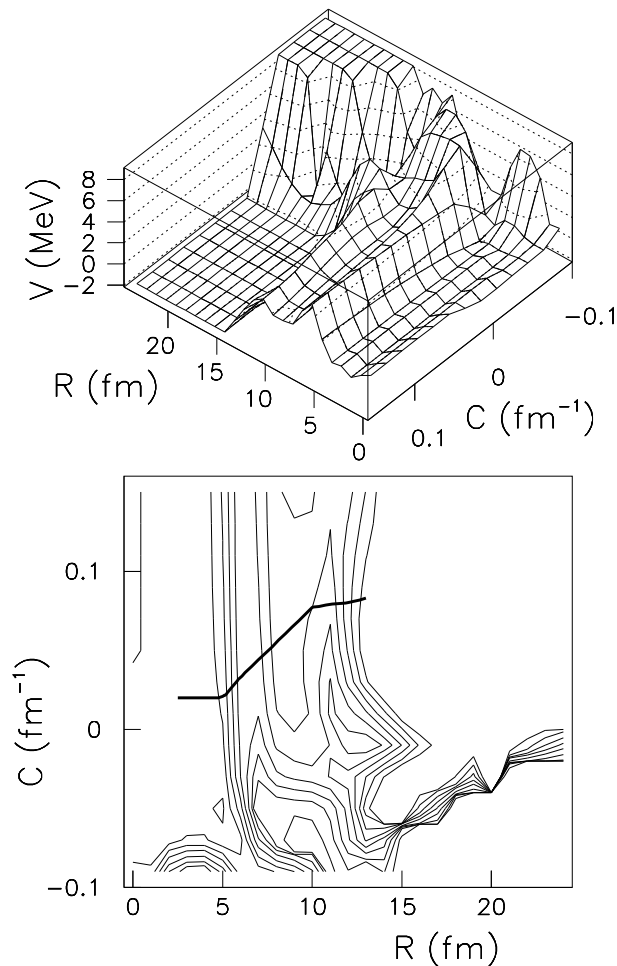


FIG. 1: Deformation energy V computed within the microscopic-macroscopic method with respect C (necking coordinate) and R (elongation). In the lower plot, the minimal action trajectory is also plotted. The step between two equipotential lines is 1 MeV.

it simply deformation energy). In Eq. (1), the inertia M is considered along a given fission path where the main coordinate is the elongation R . Therefore, for this trajectory in the configuration space, the dependencies of all generalized coordinates versus the main coordinate R are known and the quantities V and M depend only on the variables A_2 and R . The problem of finding the fission trajectory will be treated below. For a fixed combination $A = A_1 + A_2$ the deformation energy has a minimum at the charge equilibration point Z_2 , which we will not mention in the following. By definition it is defined as follows

$$V(A_2, R) = V_N(A_2, R) + V_C(A_2, R) - Q, \quad (2)$$

where $V_N(A_2, R)$ is the nuclear and $V_C(A_2, R)$ Coulomb inter-fragment potential. We also introduced the Q-value in terms of the difference between binding energies of the

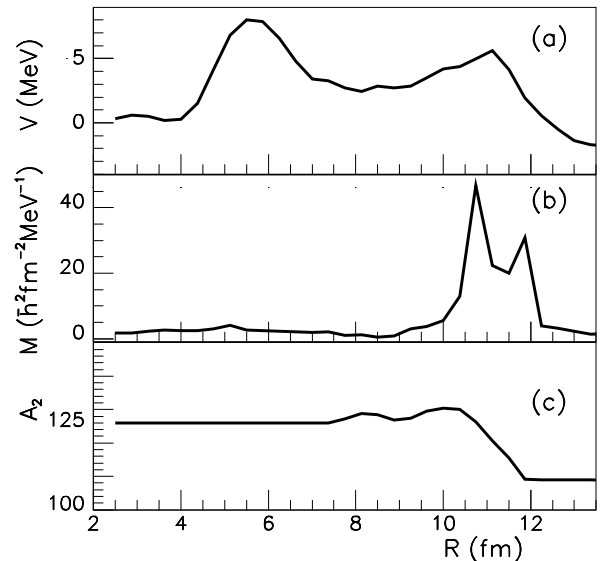


FIG. 2: (a) Adiabatic fission barrier as function of the elongation R along the minimal action path. (b) Cranking inertia as function of R . (c) The estimated A_2 during the deformation as function of R .

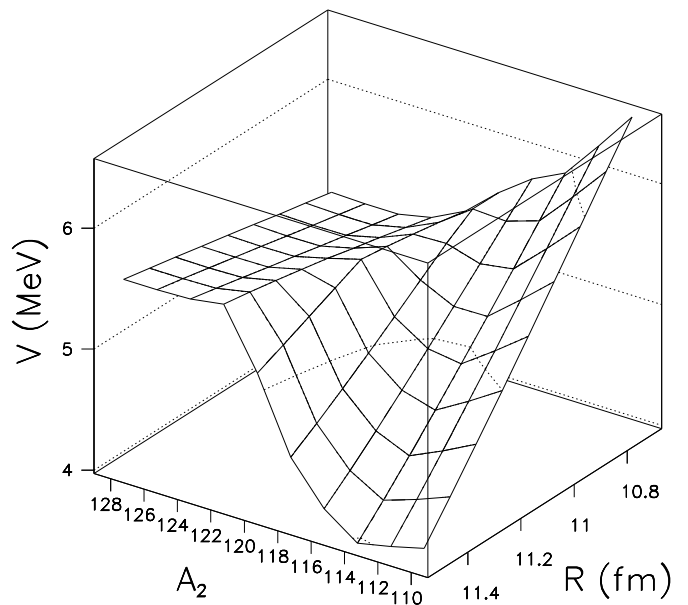


FIG. 3: Deformation energy minimized statically with respect the eccentricity of the second fragment ε_2 and the mass asymmetry parameter η as function of R and A_2 in the second saddle region.

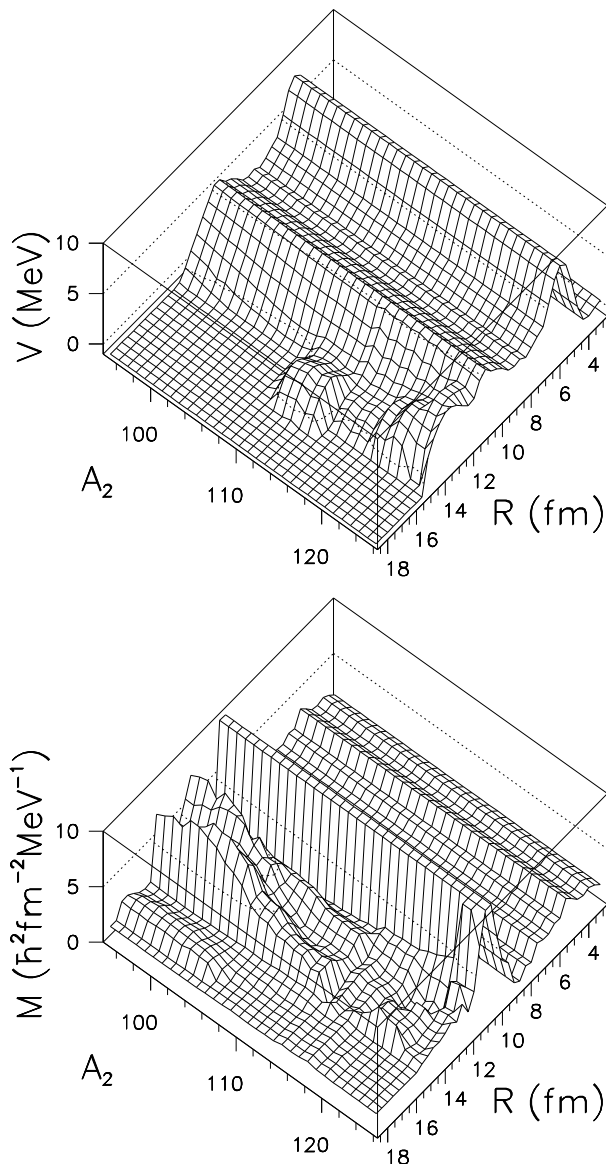


FIG. 4: Deformation energy V computed within the microscopic-macroscopic model for different binary partitions with respect A_2 and the elongation R . In the lower plot, the inertia are plotted.

parent and the sum of emitted fragments, i.e.

$$Q = B(Z_1, A_1) + B(Z_2, A_2) - B(Z, A). \quad (3)$$

For deformed nuclei, due to the fact that the largest emission probability corresponds to the lowest barrier, the deformation potential decreases in the direction of the largest fragment radius.

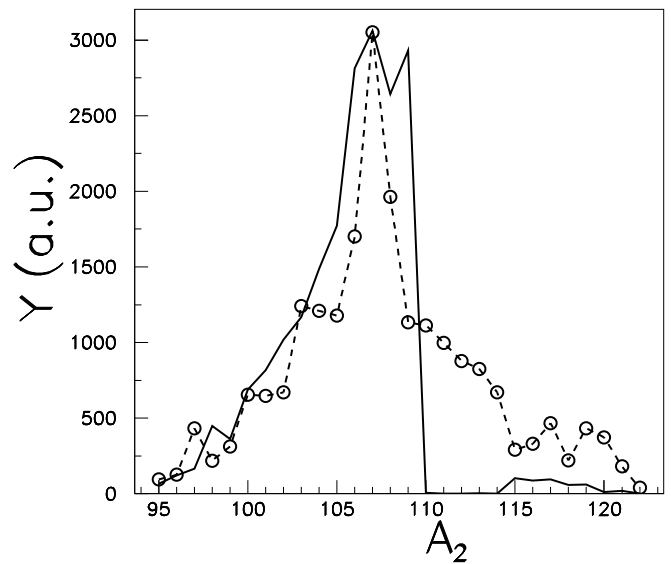


FIG. 5: Experimental yields in arbitrary units (dashed line), compared with renormalized theoretical penetrabilities calculated within the microscopic-macroscopic model (solid line) with respect to A_2 .

The deformation energy of the nuclear system is the sum between the liquid drop energy V_{LD} and the shell effects δE , including pairing corrections [19], i.e.

$$V = V_{LD} + \delta E - V_0. \quad (4)$$

The energy of the parent nucleus V_0 is used as a reference value, so that in the ground state configuration the deformation energy is zero and asymptotically, for two separated fragments at infinity, the deformation energy reaches the minus sum of energies of emitted fragments. Thus, Eq. (4) coincides with the definition Eq. (2).

The macroscopic energy is obtained within the framework of the Yukawa-plus-exponential model [20], extended for binary systems with different charge densities [21, 22]. The Strutinsky prescriptions [23] were computed on the basis of a new version of the superasymmetric two-center shell model. This version solves a Woods-Saxon potential in terms of the two-center prescriptions as detailed in Ref. [15]. The inertial parameter M is computed in the framework of the cranking model [24, 25]. We considered only cold fission process. Consequently the deformations of the final nuclei are given by their ground state values of Ref. [26].

For comparison with experimental data, the maximal values of the independent yields for a maximum excitation energy of 7 MeV were selected from Ref. [9]. The selected channels address binary partitions characterized by the following light fragments: ^{95}Rb , ^{96}Rb , ^{97}Sr , ^{98}Sr , ^{99}Y , ^{100}Y , ^{101}Zr , ^{102}Nb , ^{103}Zr , ^{104}Nb , ^{105}Mo , ^{106}Nb , ^{107}Mo , ^{108}Tc , ^{109}Mo , ^{110}Tc , ^{111}Ru , ^{112}Rh , ^{113}Ru , ^{114}Rh , ^{115}Rh , ^{116}Rh , ^{117}Pd , ^{118}Rh , ^{119}Pd , ^{120}Ag , ^{121}Cd and ^{122}Ag .

First of all, the fission path in our five-dimensional configuration space must be supplied, that is a dependence between all generalized coordinates. This trajectory starts from the ground-state of the system and reaches the exit point of the barrier. The ground-state corresponds to the minimal deformation energy in the first well. The adiabatic barrier in the multidimensional configuration space is determined by using the least action principle [23]. Therefore, a trajectory in the multidimensional space is obtained by minimizing the functional (1) by using a numerical procedure as in Ref. [15]. The deformation energy landscape, minimized versus the parameters ε_i ($i=1,2$) and a_1/a_2 , is plotted in Fig. 1 as a function of the necking coordinate C and the elongation parameter R . In the lower panel of Fig. 1 the least action trajectory is also plotted. In Fig. 2, the adiabatic fission barrier V , the effective mass M and the estimated mass number A_2 are plotted along the fission path. According to Eq. (1) the inertia is computed within the cranking approximation [24] using the expression

$$M = \sum_{j=1}^5 \sum_{i=1}^5 M_{q_i q_j} \frac{\partial q_i}{\partial R} \frac{\partial q_j}{\partial R} \quad (5)$$

where $M_{q_i q_j}$ are the elements of the inertia tensor computed for the generalized coordinates q_i and q_j . The second barrier top is located at $R=11$ fm and corresponds to a mass $A_2 \approx 120$. For a constant charge density, this ratio of the mass asymmetry addresses a heavy fragment with $A_1 - Z_1=81$ and $Z_1=51$, these values being close to magic numbers. Thus, the second saddle point corresponds to a partition that includes a double magic fragment. However, as mentioned in Refs. [27], microscopic approaches to fission [28–30] established that the second saddle point is asymmetrical with a value compatible with the observed mass ratio of the fragment distribution. Therefore, the dynamical saddle configuration obtained within our model is checked by minimizing statically the deformation energy around $R=11$ fm. The eccentricity ε_1 and the neck parameter C are kept constant. The detailed region is displayed in Fig. 3 confirming that the saddle point is located at $A_2 \approx 120$ and $R \approx 11$ fm.

Now we are interested in determining the fission barriers that address all the analyzed partitions. The asymptotic deformations of the two fragments are taken from the literature [26]. Thus, the shapes of the initial nucleus up to the second barrier and those of the final fragments are known. In order to avoid a complicated determination of the minimal action path for each partition, a linear variation from initial values of the generalized coordinates ε_i ($i=1,2$) and a_1/a_2 is postulated starting from the saddle of the second barrier configuration up to the final ones, characterizing the fragments at the end of the fission process.

By assuming a final mass asymmetry the values of the deformation energy V and the inertia M are plotted in Fig. 4 as a function of the elongation R and the light fragment mass A_2 . Some general features of the fission

barrier can be extracted. The shapes of the external barriers change dramatically upon the mass-asymmetry. For $A_2 < 110$ partitions, a double humped barrier occurs while for more symmetric channels ($A_2 > 110$) a triple humped barrier is obtained. Moreover, the exit point from the fission barrier is located at lower values of the elongation R for $A_2 < 110$ than for more symmetric channels. The inertia tends to increase when the mass asymmetry increases. It is clear that the inertia favors the production of a symmetric partition, that is $A_2 > 110$.

The spontaneous fission half-life is inversely proportional to the zero point vibration energy and to the probability of penetration through the fission barrier. If the zero point vibration energy is considered the same for all partitions, then the yields are proportional with the penetrability in each channel.

With these ingredients, the calculated penetrabilities at zero excitation energies through the barrier are compared to experimental yields in Fig. 5. We implicitly assume that the penetration of the inner barrier is the same for all partitions, so that differences in the barrier transmission between channels are induced only by the external barrier.

We obtain a very good agreement between the theoretical penetrability distribution and the experimental yields for $A_2 < 110$. The maximum theoretical value is at $A_2=107$, while the maximum experimental yield is at the same value. A sudden drop of theoretical penetrabilities is theoretically obtained for channels with $A_2 > 110$. As previously noticed, this behavior is connected with the ground state shapes of fragments that become oblate for these channels. Perhaps these oblate shapes are not the best configurations during the penetration of the barrier, and the final ground state oblate configurations are obtained only after the exit from the fission barrier.

Concluding, we computed the cold fission path in the potential energy surface of ^{252}Cf by using the two center shell model, based on the idea of the cold rearrangements of nucleons during the cold fission process. We obtained a satisfactory agreement with experimental yields, by considering variable mass and charge asymmetry beyond the first barrier of the potential surface. We can see that the mass asymmetry changed from a symmetric to the asymmetric configuration in the vicinity of the second barrier, due to the influence of the magic numbers $Z=50$ and $N=82$, i.e. $^{120}_{47}\text{Ag} + ^{132}_{51}\text{Sb}$ partition. It was shown that a good agreement with experimental data can be obtained only if the fission path proceeds through this saddle configuration. The final transmissions depend only on the external barrier and strongly depend upon the final fragment shapes. Due to the fact that prolate shapes are more favorable for the fission process, the maximal values of the yields are shifted towards channels characterized by lower values of A_2 .

Thus, the cold fission process of ^{252}Cf can be called Sn-like radioactivity, similar with the Pb-like radioactivity, corresponding to various heavy cluster emission processes. We call all these processes shortly κ (cluster)

decays. The peak in the final distribution corresponds to ^{107}Mo , due to the mass asymmetry degree of freedom, allowing a lower barrier from Sn to this nucleus.

Acknowledgments

This work was supported by the contracts IDEI-119 and PN 09 37 01 02 of the Romanian Ministry of Education and Research.

-
- [1] A. Săndulescu, R.K. Gupta, W. Scheid, and W. Greiner, *Phys. Lett.* **60** B, 225 (1976).
 - [2] A. Săndulescu, D. Poenaru, and W. Greiner, *Fiz. Elem. Chastits At. Yadra* **11**, 1334; *Sov. J. Part. Nucl.* **11**, 528 (1980).
 - [3] Yu. Ts. Oganessian, *Nucl. Phys. A* **685**, 17c (2001).
 - [4] R.K. Gupta, C. Parvulescu, A. Săndulescu, and W. Greiner, *Z. Phys. A* **283**, 217 (1977).
 - [5] R.K. Gupta, A. Săndulescu, and W. Greiner, *Phys. Lett.* **67** B, 257 (1977).
 - [6] S. Hofmann and G. Münzenberg, *Rev. Mod. Phys.* **72**, 733 (2000).
 - [7] S. Hofmann, G. Münzenberg, and M. Schädel, *Nucl. Phys. News* **14** No. 4, 5 (2004).
 - [8] Yu. Ts. Oganessian, *et. al.* *Nucl. Phys. A* **734**, 109 (2004).
 - [9] F.-J. Hamsch, H.-H. Knitter, and C. Budtz-Jorgensen, *Nucl. Phys. A* **554**, 209 (1993).
 - [10] H.-H. Knitter, F.-J. Hamsch, and C. Budtz-Jorgensen, *Nucl. Phys. A* **536**, 221 (1992).
 - [11] A. Sandulescu, A. Florescu, F. Carstoiu, W. Greiner, J.H. Hamilton, A.V. Ramayya, and B.R.S. Babu, *Phys. Rev. C* **54**, 258 (1996).
 - [12] A. Săndulescu, Ș. Mișicu, F. Carstoiu, A. Florescu, and W. Greiner, *Phys. Rev. C* **57**, 2321 (1998).
 - [13] F. Gonnemann, and B. Borsig, *Nucl. Phys. A* **530**, 27 (1991).
 - [14] D.S. Delion and A. Săndulescu, *Rom. J. Phys.* **52**, 43 (2007).
 - [15] M. Mirea, *Phys. Rev. C* **78**, 044618 (2008).
 - [16] M. Mirea, D.S. Delion, and A. Sandulescu, *EPL* **85**, 12001 (2009).
 - [17] M. Mirea, *Phys. Lett. B* **680**, 316 (2009).
 - [18] G. Gamow *Z. Phys.* **51**, 204 (1928).
 - [19] J.R. Nix, *Ann. Rev. of Nucl. Sci.* **22**, 65 (1972).
 - [20] K.T.R. Davies, and J.R. Nix, *Phys. Rev. C* **14**, 1977 (1976).
 - [21] D.N. Poenaru, M. Ivascu, and D. Mazilu, *Comput. Phys. Commun.* **19**, 205 (1980).
 - [22] M. Mirea, O. Bajeat, F. Clapier, F. Ibrahim, A.C. Mueller, N. Pauwels, and J. Proust, *Eur. Phys. J. A* **11**, 59 (2001).
 - [23] M. Brack, J. Damgaard, A. Jensen, H. Pauli, V. Strutinsky, and W. Wong, *Rev. Mod. Phys.* **44**, 320 (1972).
 - [24] M. Mirea, R.C. Bobulescu, and M. Petre, *Rom. Rep. Phys.* **61**, 646 (2009).
 - [25] M. Mirea, and R.C. Bobulescu, *J. Phys. G*, in press (2010); Preprint arXiv:0909.2098v1 [nucl-th] (2009).
 - [26] P. Möller, J.R. Nix, W.D. Myers, and W.J. Swyatecki, *At. Data Nucl. Data Tables* **59**, 185 (1995).
 - [27] J.P. Bocquet, and R. Brissot, *Nucl. Phys.* **A502**, 213c (1989).
 - [28] M. Mirea, L. Tassan-Got, C. Stephan, C.O. Bacri, and R.C. Bobulescu, *Phys. Rev. C* **76**, 064608 (2007).
 - [29] J.F. Berger, M. Girod, and D. Gogny, *Nucl. Phys.* **A438**, 23c (1984).
 - [30] P. Moller, and A. Iwamoto, *Phys. Rev. C* **61**, 047602 (2000).